

13,14

a-C:ND coatings obtained by plasma chemical deposition: interplay between field emission properties and phase composition

© I.A. Zavidovskiy, O.A. Streletskiy, A.A. Tatarintsev, K.F. Minnebaev, A.A. Khaidarov

Moscow State University,
Moscow, Russia

E-mail: ia.zavidovskii@physics.msu.ru

Received December 18, 2022

Revised December 18, 2022

Accepted January 24, 2023

The coatings comprised of the nanodiamond-based and amorphous-carbon-based phases (a-C:ND coatings) are investigated. The a-C:ND coatings were synthesized by chemical vapor deposition in the arc discharge plasma (by plasma chemical deposition) at various concentrations of Ar/H₂/CH₄. Raman spectroscopy showed that, apart from the diamond substructure, studied coatings contain amorphous-carbon-based and polyene-based phases, while diamond phase is passivated by hydrogen to different degrees. The interplay between the deposition parameters and materials' structure is analysed. It was shown that the ordering of the amorphous substructure and the formation of the phase boundaries affect the electron transport and secondary electron emission properties. The subject of the investigation of the true secondary electron spectra for the analysis of the nanostructured carbon materials is analysed. It was shown that the change of the polyene fraction in the structure of the samples leads to the variation of the ratio of field emission and thermionic emission. The influence of the structure and phase composition of the samples on their electron emission properties is investigated. In particular, their effect on the turn on field, which value varied in the 9–18 V/μm range for the studied samples, is analysed.

Keywords: nanodiamond composites, polyene-like materials, electron transport, hydrogen passivation, turn-on field.

DOI: 10.21883/PSS.2023.04.56008.556

1. Introduction

Electron emission of carbon materials is being extensively studied nowadays [1–5]. In doing this, the development of practical applications of the nanostructured carbon is connected with the investigation of both the field electron emission [1–3] and the secondary electron emission [4,5]. The method of chemical vapor deposition (CVD) is often used to synthesize carbon-based materials that are characterized by dependence on the structure of both low secondary electron emission [6] and high [7] secondary electron emission, as well as to form high-performance thermo-electron emitters [8] and field emitters [9].

The effective field emission of nanostructured carbon materials is considered to be connected with the combination of the negative electron affinity of hydrogen-passivated diamond and the formation of a conductive structure based on sp²-carbon, which ensures the transfer of electrons to the emitting surface [10]. At the same time, a number of studies are devoted to the investigation of multistage processes of diamond-based material processing: thus, in [8] the formation of a conductive structure in the diamond by means of laser radiation is considered, in [11] the possibility of silver ion implantation initiating the graphitizing of diamonds is analyzed, and in [12] it is shown, that emission characteristics of doped diamond can be improved via a multistage process that includes processing by oxygen plasma and coating of the structure with a layer of caesium.

However, an increase in the number of stages of material formation has an adverse effect on the availability of these materials and the scalability of their production.

It is worth noting that both the PVD process (physical vapor deposition) and the CVD process allows for the formation of structures with nanodiamond and amorphous phases (a-C:ND-structures) by single-stage process with properties of these structures changing significantly depending on variations of deposition parameters [13–16]. In [15] it is shown, that nanodiamonds embedded in an amorphous carbon matrix can be formed by magnetron sputtering of a nanodiamond target. At the same time, according to [15], properties of such coatings are dependent on the deposition time due to the effect of plasma on the target. This makes it difficult to create coatings with required parameters and thickness using PVD techniques.

As a consequence, it is interesting to study the structure of a-C:ND-composites produced by CVD methods. Also, an actual task is the analysis of emission characteristics of such structures: thus, in [17] it is shown, that good emission properties of these structures can be provided not only by the emission from the diamond surface but also from sp²-hybridized interfaces. Due to this circumstance, a comprehensive analysis of such structures is of interest as it allows identifying the connection between the structure of the hybridized component and the emission properties.

a-C:ND-coatings in this study were produced by chemical vapor deposition in arc-discharge plasma (plasma-

chemical deposition) at different partial vapor pressures in the working chamber atmosphere. The under-study method of deposition belongs to CVD methods, however, in comparison with non-plasma-assisted CVD methods, it has advantages of low deposition temperature [18], high deposition rate and, as a consequence, relatively low energy and time costs [19]. The structure of synthesized material was analyzed by methods of x-ray diffraction, scanning-electron microscopy (SEM), Raman scattering spectroscopy (Raman spectroscopy). Characteristics of the secondary electron emission (SEE) of samples were considered that allowed obtaining the information about properties of the electron transport. The obtained information allowed identifying the relation between conditions of the deposition, characteristics of the electron emission of samples in electric field and phase composition, disordering and hydrogen passivation of diamond crystallites.

2. Materials and methods

2.1. Preparation of samples

Samples for the study were produced by the method of plasma-chemical deposition of carbon from gaseous phase with arc discharge in the atmosphere of hydrogen, argon and methane mixture. Schematic diagram of the deposition process is shown in Fig. 1.

Substrates in the form of *n*-type silicon plates (Fig. 1, 5) were located behind the anode (4) on the substrate holder (6) with the indirect heater (7) allowing for heating up to 1000°C. The arc discharge (3) was initiated between the cathode made in the form of graphite rod (2) installed in the molybdenum holder (1) and the anode (4) made in the form of copper disc. Coatings were deposited at a working pressure of 60 Torr, the discharge current was 1 A, the discharge voltage was 700 V. The insert in Fig. 1 shows the process of coating deposition. Temperature of the substrate holder was measured by a chromel-copel thermocouple

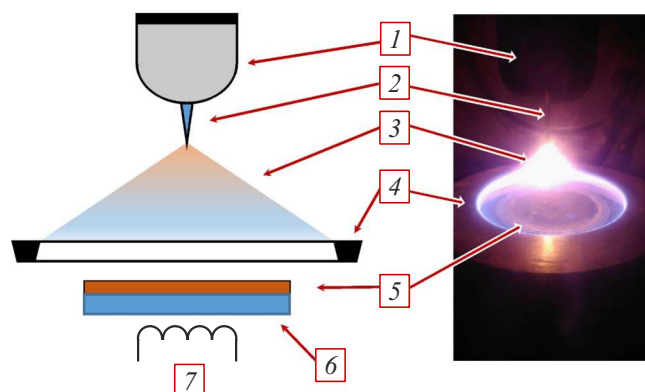


Figure 1. Set-up and photo of the process of a-C:ND film deposition. 1 — molybdenum holder of the cathode; 2 — graphite cathode; 3 — discharge; 4 — anode; 5 — substrate; 6 — substrate holder; 7 — heater.

installed inside the holder and was equal to 700°C. The coatings were produced in three modes at different relative concentrations of gases in the working chamber, which are denoted as I, II and III in the following text. For I, II and III modes the H₂:Ar:CH₄ ratio was 86.5 : 10 : 3.5, 77.5 : 20 : 2.5 and 87.5 : 10 : 2.5, respectively. Thickness of the coatings was determined at the cleavage edge of the silicon plate and was equal to 1 μm for all sample series.

2.2. Analysis of samples

X-ray diffraction. X-ray diffraction analysis (XRD analysis) of samples was carried out using a D/MAX 2500 diffractometer by Rigaku.

SEM. Surface of samples was studied by a LEO 1455VP scanning electron microscope with an accelerating voltage of 10 keV. The secondary electrons were collected by an Everhart-Thornley detector.

Raman spectroscopy. Raman scattering spectra were obtained using a Sunshine GE-Raman spectrometer combined with a Leitz Wetzlar microscope. The laser excitation wavelength was 532 nm, the laser power was 1 mW. Spectra were measured using a ×50 lens (with a numerical aperture of N.A. = 0.85). Samples were measured over 3–5 regions on the surface and the most typical spectrum was selected for the analysis of each sample. Results of the scanning were processed by the MagicPlot software package.

SEE. The energy dependence of SEE for the produced samples was studied using a LEO 1455VP scanning electron microscope at different energies of the primary electron beam. The set-up to measure energy spectrum based on the toroidal electron spectrometer is described in [20,21]. The secondary electrons were measured as follows: the primary electron beam was directed to a Faraday cylinder, which was used to determine the total flux of primary electrons, then the beam was moved to a pre-defined coordinate on the plane where the under-study sample was located. In the course of the experiment the current of secondary electrons was detected by a hemispherical collector with aquadag coating on its inner side. The secondary electron emission coefficient was determined by the ratio of the collector current to the current measured on the Faraday cylinder. Currents were measured by Keithley 6485 nanoammeters.

Electron emission under electric field. Characteristics of the field emission were measured in ultrahigh vacuum conditions using a Lass-4000 system by Riber at a pressure not higher than 10⁻⁹ Torr.

The initial sample was installed on the cathode made of a polished stainless steel plate. The cathode and the sample were located at a distance of 300 μm from the anode, which was made of a polished stainless steel plate as well. A special polytetrafluorethylene separator was installed between the cathode and the anode. The separator was located in such a way as to ensure a working emitting area of 0.2 cm² and a distance between electrodes of 300 μm.

A voltage from 0 to 7 kV was applied to the anode. The current was measured by a Tektronix DMM 4050 nanoammeter combined with a personal computer.

3. Results and discussion

3.1. X-ray diffraction

Fig. 2 shows the results of XRD analysis for sample I. The presented diffraction pattern was typical for all the samples under study. Two peaks at $2\Theta = 44.0^\circ$ and 75.4° correspond to interplanar distances of 2.06 and 1.26 Å respectively. The positions of lines like these are typical for both the disordered carbon with high content of sp^3 -hybridized atoms [22] and the polycrystalline diamond [23]. At the same time, width of the peaks in question is more typical for crystalline samples, suggesting that the sample has a phase based on diamond crystallites. In addition to the peaks shown in Fig. 2, an intensive maximum corresponding to an interplanar distance of 2.7 Å was observed in diffraction patterns. This peak corresponds to the line (002) of silicon [24] and is due to the contribution from the silicon substrate.

It is worth noting that the interplanar distance of 2.06 Å is typical for the line (111) of diamond, although both the peak (110) of graphite at 1.23 Å and the peak (220) of diamond at 1.26 Å [22] can present near the position of 1.26 Å in carbon materials. Due to this fact, the line (111) of diamond was selected to determine the size of crystallites by Scherrer formula [25]. The estimate by Scherrer formula has shown that the crystallite size of diamond is about 10 nm. However, the method of X-ray diffraction is not always sufficient for the analysis of samples that contain several carbon-based phases: thus, in [26] the diffraction pattern of a-C:ND-composites has only shown the presence of two peaks related to diamond crystallites, however the X-ray photoelectron spectroscopy analysis has shown that the percentage of „diamond“ hybridizing atoms (the ratio of intensities of $sp^3/sp^3 + sp^2$ lines) was as low as 41%.

3.2. SEM

Fig. 3 shows SEM-images of samples. For sample I, a formation of large irregularities with sizes of 25–50 μm on the film surface is observed. The formation of these features takes place in a non-uniform manner over of coating area. Samples II and III are characterized by morphological features with sizes of 3–6 and 3–15 μm, respectively, which are distributed over the surface in a quite uniform manner. It is worth noting that the size of irregularities observed by SEM is several orders of magnitude higher than the typical size of the diamond component (see section 3.1). Thus, morphological features of films are directly related to the sp^3 -component of structures under study. This suggests that the sample under study contains non-diamond carbon-based phases in addition to the diamond component. To analyze them, the Raman spectroscopy is often used.

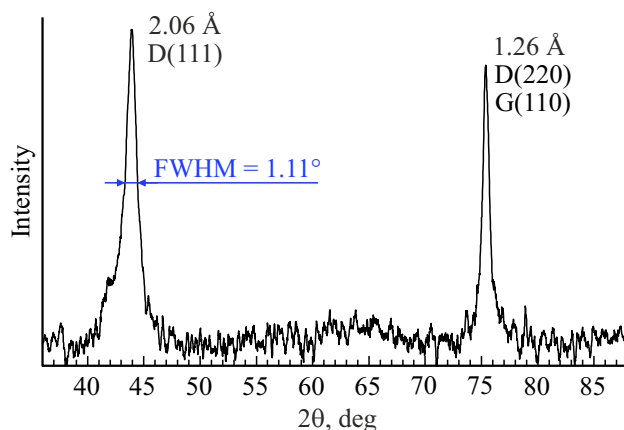


Figure 2. Results of photometering of typical X-ray diffraction of samples. Positions of peaks in interplanar distance units, lines attributing and full width at half maximum for the 44.0° peak are marked.

3.3. Raman spectroscopy

Fig. 4 shows Raman spectra of samples under study. These spectra are characterized by quite intensive D-lines and G-lines with their maxima at 1343–1349 and 1555–1558 cm^{-1} , respectively. The presence of D-peaks and G-peaks is typical for disordered carbon materials [27]. In the vicinity of D-peaks and G-peaks, less intensive lines with maxima at 1010–1130, 1158–1200 and 1343–1349 cm^{-1} are observed. Similar spectra have been considered in [28,29], where it was shown that the presence of additional lines is related to the presence of different polymer substructures in the material. In turn, lines in the range of 2500–3000 cm^{-1} may be related both to the presence of second orders of D-lines and G-lines and to C–H-bonds [30].

To consider Raman spectra in more detail, the MagicPlot software was used to expand the spectra to Gaussian–Lorentzian components. Results of the expansion are presented in Table 1.

First of all, to interpret the data, it is worth noting that the emergence of a D-peak is related to the breathing mode of sp^2 -hybridized clusters, which is manifested in Raman spectra of disordered structures. At the same time, the presence of a G-peak is due to the excitation of stretching vibrations of the sp^2 -hybridized carbon [31]. Thus, the lines in question are mainly related to the graphitized component of films. This is confirmed by the theoretical analysis showing that the Raman response of diamond is two orders of magnitude lower than that of graphite [32]. Also, it is confirmed by the consideration of a-C:ND-structures, which Raman spectra were determined mainly by the amorphous component [15]. In turn, the quantum-chemical analysis of Raman response of diamond crystallites has shown that in the case of hydrogen-passivated clusters, a number of Raman lines related to vibrations of C–C-bonds and C–H-bonds may be manifested in the range of

Table 1. Results of spectra expansion: positions of peaks, k ; full width at half maximum (FWHM); intensity of peaks related to the sum intensity of all spectral components in the range under study

	Polyenic C–C (1)	Polyenic C–C (2)	D-Line D	Polyenic C=C	D-Line G	2D-Line 2D	C(sp ³)-H _x
Sample I							
k , cm ⁻¹	1130	1200	1349	1462	1549	2700	2950
FWHM, cm ⁻¹	56	94	162	82	106	691	599
Relative intensity, %	3	2	20	6	8	47	14
Sample II							
k , cm ⁻¹	1130	1200	1349	1453	1545	2700	2950
FWHM, cm ⁻¹	52	130	129	79	117	437	494
Relative intensity, %	4	7	32	11	18	13	14
Sample III							
k , cm ⁻¹	1010	1158	1343	1469	1562	2700	2950
FWHM, cm ⁻¹	86	94	162	84	126	410	366
Relative intensity, %	1	8	36	7	24	15	9

1000–1500 cm⁻¹ [33], however, the only specific line for the sp³-carbon is a narrow line in the vicinity of 1332 cm⁻¹, which intensity is relatively low in the case of a-C:ND-structures. Thus, no contribution of the diamond component of coatings is observed in the Raman spectra investigated in this study, which is correlated with the literature data.

It is worth noting that positions of D-lines and G-lines of samples I–III are different from each other insignificantly. This is evidence that the ratio of the sp²/sp³-hybridized carbon in the amorphous component of coatings under study undergoes no significant changes. However, it is difficult to evaluate this ratio due to the multicomponent structure of coatings and the variability of the ratio of D-lines and G-lines intensities (I_D/I_G), which complicates the consideration of spectra in accordance with the „amorphization trajectory“ [34]. The variation of I_D/I_G may be due not only to the change in the sp²/sp³-ratio [35] but also to the variation of degree of ordering of the amorphous component [36,37]. The behavior of changes in this value is considered in the following text.

The presence of lines in ranges of 1010–1200 and 1453–1462 cm⁻¹ is indicative of the presence of a component in the film structure, which is based on polymers containing C–C-bonds and C=C-bonds, which vibrations cause the emergence of these lines. Thus, in [28,29] the emergence of similar lines was attributed to the formation of trans-polyacetylene and poly(p-phenylene vinylene). For the carbon coatings produced by the CVD method, similar peaks, in general, are considered as related to the formation

of polyenes, i.e. conjugated polymers that contain at least three alternating double and single C–C-bonds, which the trans-polyacetylene belongs to [38]. At the same time, as it has been shown in [39], positions of peaks in spectra of polyene-containing amorphous carbon are different from the maxima observed in spectra of the pure trans-polyacetylene, that may be evidence of the presence of impurity atoms, –CH_x-groups and cis-isomer fragments in the structure of the polymer component. In turn, the presence of two typical peaks in the range of 1010–1200 cm⁻¹ may be indicative of the presence of several types of polymers in the structure [28,29]: this issue needs further investigation for the structure in question.

The wide plateau of the peak within 2100–3500 cm⁻¹ is indicative of the fact that this line can be fitted by several Gaussian components. In [30] it is shown, that components of similar peaks may include second orders of D-lines and G-lines (2D-lines and 2G-lines), as well as lines corresponding to the vibration of C–H_x-bonds. Positions of lines corresponding to 2D and 2G for the structures under study are at 2700 and 3100 cm⁻¹. At the same time, positions of the lines corresponding to C–H_x-bonds vary depending on the carbon atom hybridization: thus, for the sp³-hybridized atom this peak is positioned in the range of 2800–2950 cm⁻¹, and for the sp²-hybridized atom this peak has maximum at 2980–3060 cm⁻¹. Due to the fact, that in the spectra under study the region where wave number exceeds 3000 cm⁻¹ is out of the prominent plateau (2600–2900 cm⁻¹), a conclusion can be made that

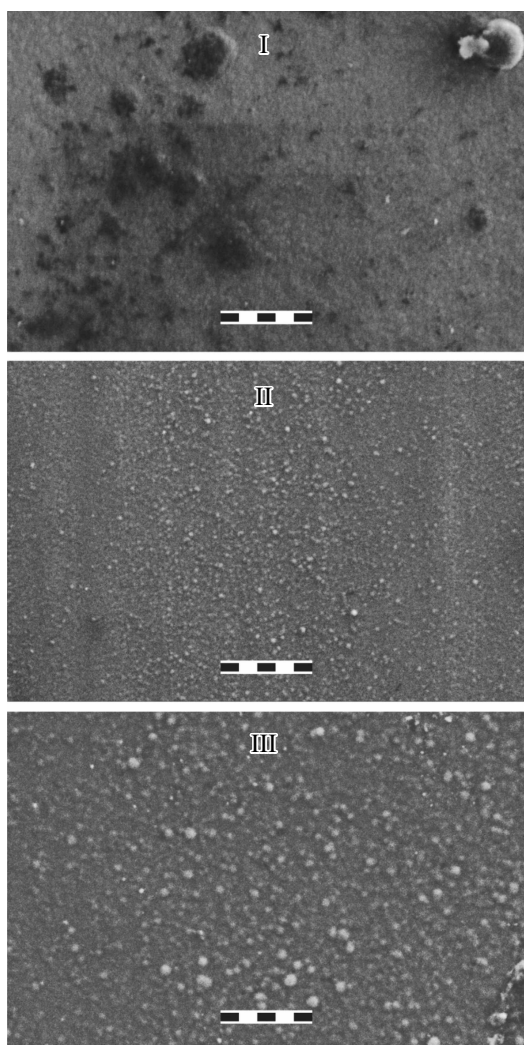


Figure 3. SEM-images of samples. The scale bar has a length of 10 μm .

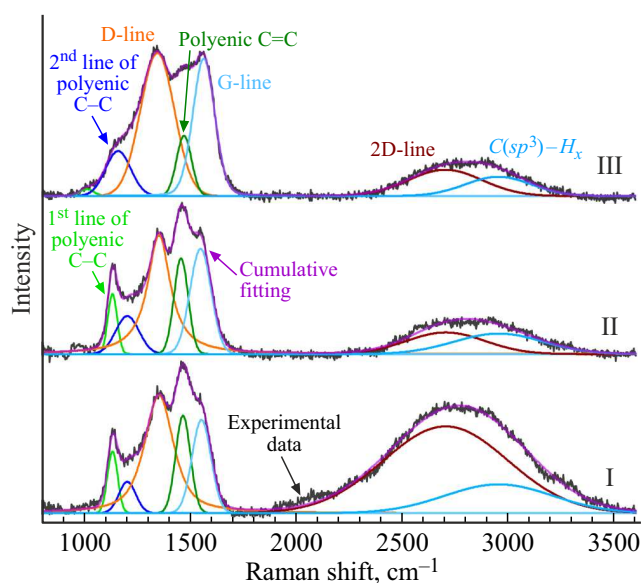


Figure 4. Raman spectra of samples under study and their expansion to Gaussian–Lorentzian components.

Table 2. Ratio of intensities of I_D , $I_{\text{polyenic C=C}}$, $I_{C(\text{sp}^3)\text{-H}}$ components of Raman spectra to I_G

	I_D/I_G	$I_{\text{polyenic C=C}}/I_G$	$I_{C(\text{sp}^3)\text{-H}}/I_G$
I	2.59	0.82	1.76
II	1.84	0.61	0.82
III	1.51	0.28	0.40

2G-peaks and $C(\text{sp}^2)\text{-H}_x$ -peaks in the spectra under study have a relatively low intensity and can be neglected in the expansion. Due to this, 2D-line and $C(\text{sp}^3)\text{-H}_x$ line with their positions recorded at 2700 and 2950 cm^{-1} were selected as fitting components for the spectrum section of 2100–3500 cm^{-1} . The position of $C\text{-H}_x$ was selected from the range of 2800–2950 cm^{-1} because of the best fitting of experimental spectra.

Low intensity of the 2G-line as compared with the 2D-line is typical for carbon materials [40–42]. At the same time, the greater intensity of the $C(\text{sp}^3)\text{-H}_x$ line as compared with the $C(\text{sp}^2)\text{-H}_x$ line may be indicative of the fact that in the structure of samples under study nanodiamond crystallites are the most susceptible to the hydrogen passivation.

The analysis of Raman-spectra shows that samples contain phases based on polyenes and amorphous carbon. In turn, the nanodiamond component detected by the X-ray diffraction method is hydrogen-passivated according to the results of Raman-spectroscopy. Thus, the most important quantitative characteristics of spectra that allow for identification of the change in the degree of disordering of the amorphous component, the ratio between polyene and amorphous carbon phases, as well as the character of the hydrogen passivation are I_D/I_G , the ratio of intensities of the line of polyene $C=C$ -bonds vibrations and the G-line ($I_{\text{polyenic C=C}}/I_G$), as well as the ratio of intensities of $C(\text{sp}^3)\text{-H}$ -line and G-line ($I_{C(\text{sp}^3)\text{-H}}/I_G$). These values are given in Table 2.

It is worth noting that the G-line intensity is proportional to the number of sp^2 -bonds in the sample structure [43], thus its value is often used as a reference for the analysis of change in various spectral components [44,45].

Thus, the information considered in sections 3.1 and 3.3 is indicative of the fact that a-C:ND-samples are hydrogen-passivated diamonds with a size of about 10 nm, which are dispersed in a matrix containing amorphous carbon and several phases based on polyene-like structures. The sample I has most prominently manifested hydrogen passivation, disordering of the amorphous matrix and the percentage of polyene-like inclusions in the material structure. These effects are manifested in a medium degree in the sample II and manifested in the lowest degree in the sample III.

3.4. Discussion of structural features of coatings

To establish the interrelation between the structure of coatings produced at different partial pressures of gases and

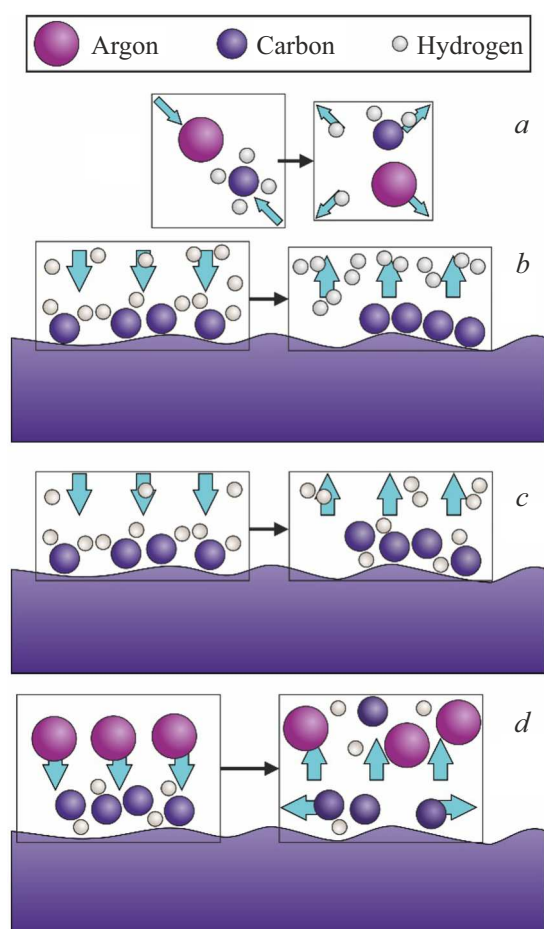


Figure 5. Typical processes having effect on the coating structure. Inserts show typical situations before and after the interaction of particles. *a*) Ionization of gases during the interaction with argon. *b, c*) The process of hydrogen etching out of the $-C_xH_y$ -radicals deposited onto the surface, that results in the formation of (*b*) diamond component or (*c*) polyene-like component. *d*) The effect of argon leading to material sputtering and greater surface diffusion.

under different conditions of the deposition, it is necessary to consider roles of the gases used in the plasma-assisted CVD process. These roles are schematically shown in Fig. 5. Thus, Fig. 5, *a* shows a typical feature of the plasma-assisted CVD method, which consists in the argon plasma interaction with molecules of hydrocarbons and hydrogen resulting in their dissociation and ionization [46,47], which, in turn, increases chemical activity of components of the working atmosphere. The role of methane and its derivatives (C_xH_y) is demonstrated in Fig. 5, *b* and *c*: deposition of hydrocarbons on the film surface is the source of material for its growth. And the etching of hydrogen from the surface of the growing film takes place mainly during the interaction of $-C_xH_y$ -radicals with the atomic hydrogen [47], which is schematically shown in Fig. 5, *b* and *c*. In this case the reactive atomic hydrogen is formed as a result of dissociation of not only molecular

hydrogen but also of methane [48]. The difference in behavior of the process of hydrogen removal shown in Fig. 5, *b* and *c* reflects the fact that the different balance between the rate of deposition of hydrocarbons and the „annealing“ of hydrogen leads to the formation of different structures that can be sp^3 -hybridized (Fig. 5, *b*) or polyene-like (Fig. 5, *c*). In the case, when hydrogen is not completely removed from the material in the process of synthesis, depending on the process dynamics, it can form not only a polymer substructure but also a hydrogen passivation at the boundary of diamond crystallites [49,50]. Also, an incomplete process of the $sp^2 \rightarrow sp^3$ -rearrangement induced by the atomic hydrogen may also result in the formation of a disordered graphitized component, however, this process, as a rule, can not be described within the framework of simple considerations [50].

In turn, for the plasma-assisted CVD running in an argon-containing working atmosphere, also a certain role can be played by the manifestation of processes related to the interaction of argon particles with the surface. Thus, in [46] it is shown that the addition of argon promotes formation of crystallite nucleation centers. This effect is similar to the effect of ion assistance within the PVD method: thus, it is known that irradiation by low-energy Ar^+ ions in the process of depositing promotes the formation of defects on the surface of the growing film, which are preferable nucleation centers [39,51,52]. At the same time, as it is shown in [52], the defect formation of the ion assistance is accompanied by the selective sputtering of loosely bound components of the material and the stronger surface diffusion of adsorbed atoms and nuclei. These processes are schematically shown in Fig. 5, *d*. The energy of the C–H-bond for a hydrocarbon structure is 3.7 eV [53], the displacement energy of the sp^2 -hybridized carbon atom is 25 eV, and the displacement energy of the sp^3 -hybridized carbon atom is 80 eV [54], hence a hydrogen atom can be removed not only by the action of the atomic hydrogen of the gaseous phase but also by the selective sputtering by argon particles. At the same time, according to [52], different manifestation degree of processes of defect formation and strengthening of surface diffusion can result in both the graphitization and the increase in percentage of the sp^3 -component. It is known that the contribution of defect formation prevails for the plasma-assisted CVD in the case of argon irradiation [55]. It seems that because of the above circumstance the increase in the relative concentration of argon in the course of plasma-assisted CVD process results in disordering of the material [56].

It is worth to note that the description presented in this section does not take into account the difference in behavior of the material deposition process and the processes of interaction of gases under varying pressures of the working mixture and varying temperatures of the substrate. The purpose of this study is to identify the relationship between the composition of working gas and the structure of coatings. Hence, the variation of other parameters and the studying of their effect on the structure

of material should be the subject of analysis of further studies.

The presented consideration makes it possible to conclude that coating I produced with the highest concentration of methane and the lowest concentration of argon is characterized by a low degree of „annealing“ of the hydrogen component and a low effect of the argon flux. Due to this, the structure of coatings has a relatively high level of hydrogen that is presented in both the polyene phase and the hydrogen-passivated diamond phase; at the same time, the low contribution of the assistance of argon ions results in the situation that the manifestation of the defect-induced nucleation and the strengthening of the surface diffusion is less prominent, therefore coating I is characterized by a greater size of non-uniformly located morphological features. In coating II produced with the highest concentration of argon, the formation of relatively low surface irregularities with a small size is observed, which is indicative of a considerable contribution of the ion-induced sputtering and the nucleation. Coating III produced with a high concentration of hydrogen is characterized by small morphological features with a wider distribution as compared with sample II; at the same time, the percentage of polyene phase and the degree of passivation of sample III is higher than that of sample II. Thus, the interaction of argon with the surface is more effective in the creation of nucleation centers than the hydrogen irradiation, however, the chemical mechanism of hydrogen etching in the course of interaction with atomic H is more effective than sputtering of relatively loosely-bound hydrogen by argon ions.

It is worth noting that the disordering of the amorphous phase of coatings changes with variation of deposition parameters, which is evidenced by variation of the I_D/I_G ratio in Raman-spectra. The increase in I_D/I_G is correlated with the increase in $I_{\text{polyenic C=C}}/I_G$ (i.e. with the growth of the polyene phase fraction) and in $I_{\text{C(sp}^3\text{)-H}}/I_G$ (i.e. with the growth of hydrogen passivation of diamonds). At the same time, it is known that an increase in hydrogenation of the amorphous carbon decreases the I_D/I_G [35,57], therefore a change in the I_D/I_G can not be described by embedding hydrogen into the amorphous phase of coatings. It is likely that in the case under study the disordering of amorphous substructure is affected by the growth of the polyene phase percentage, which leads to an increase in the area of boundaries between the amorphous component and the polymer component that manifests in spectra as a disordering of the material.

3.5. Secondary electron emission

The secondary electron emission of carbon materials often becomes a subject of studying because of its variability that allows finding different applications for carbon-based coatings related to SEE [58,59]. Thus, amorphous films with low secondary electron yield, $\text{SEY} \approx 1.1$ are suggested for the use as coatings for synchrotron components to decrease the electron-stimulated desorption, the transverse expansion

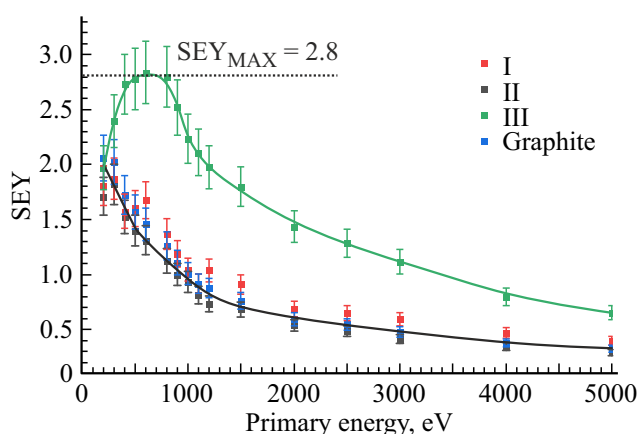


Figure 6. The secondary electron yield (SEY) as a function of energy of the primary electron beam. Black line reflects the dependence typical for HOPG and samples I, II.

of charged particle beam and to decrease the thermal load on cryogenic vacuum systems and the loss of beam particles [58]. In turn, coatings based on the nanocrystalline diamond with $\text{SEY} \approx 10$ can be used as elements of electron multipliers and photomultipliers. The applicability of carbon materials in different SEE-related applications is determined by the structure of material. The most illustrative characteristic, which is dependent on the material structure to a significant extent, is the dependence of SEE on the energy of the primary electron beam. The higher is the beam energy where maximum SEY is observed, the longer is free path of secondary electrons and, as a consequence, the lower is manifestation of the electron scattering effect. It has been shown for the carbon materials with composition determined by a single phase, that the cross-section of secondary electrons interaction with sp^2 -hybridized atoms is considerably higher than the cross-section of secondary electrons interaction with sp^3 -carbon [59]. However, in the case of structures composed of several phases the transfer of electrons can be affected by the electron scattering at the interfaces [60,61].

The dependence of SEE on the energy of the primary beam, recorded for the samples under study is shown in Fig. 6. Highly-oriented pyrolytic graphite (HOPG) was used as a reference sample (ZYB-type highly-oriented pyrolytic graphite with a plane misorientation angle of $0.8 \pm 0.2^\circ$ manufactured by „NT-MDT“ LLC). The results obtained for graphite are consistent with the literature data [62,63]. However, the data of [62,63] indicates that the experimentally obtained dependencies of this study have failed to identify the maximum SEY (SEY_{MAX}) observed for the electron energy of ~ 100 eV.

The energy SEYs of samples I and II in the measured range are similar to the dependencies obtained for graphite, however, SEY of sample III is considerably different from the data obtained for other samples. SEY_{MAX} of sample III is observed for electrons with an energy of 600 eV, its value

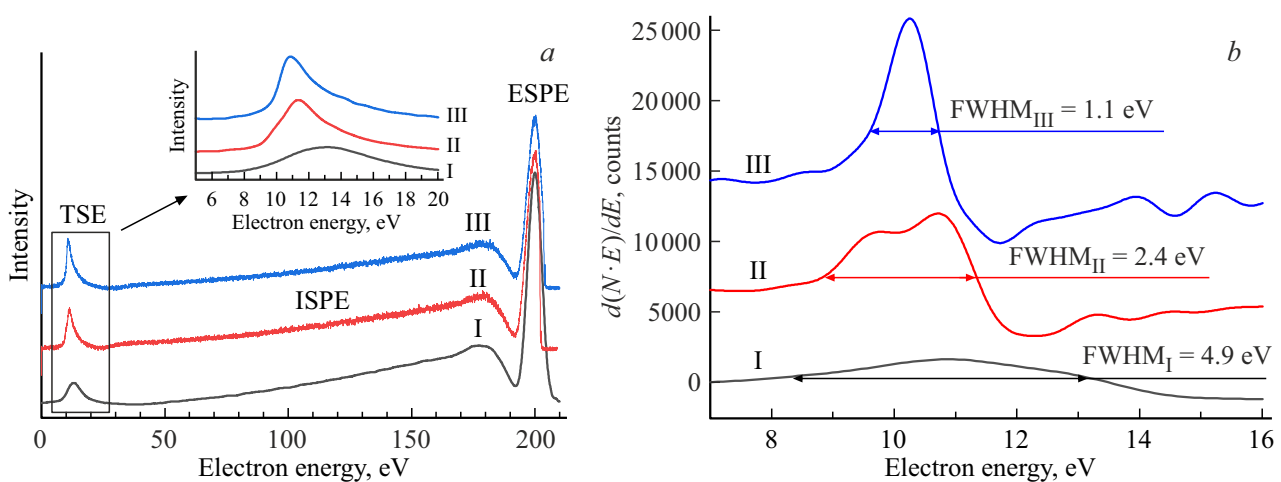


Figure 7. a) Spectrum of secondary electrons for the samples (shown with Roman numerals), irradiated by the primary beam with an energy of 200 eV. Regions of true secondary electrons (TSE), inelastically scattered primary electrons (ISPE), elastically scattered primary electrons (ESPE) are shown. The insert shows smoothed spectrum of true secondary electrons. b) $d(N \cdot E)/dE$ differential and widths of peaks.

is 2.8. At the same time, SEY_{MAX} for the polycrystalline diamond exceeds 10 and this maximum is observed for electrons with energies greater than 1000 eV [64]. The information about SEE of the samples under study is indicative of the fact that phases based on disordered carbon and polyenes in them have a significant effect on the electron emission and electron transport, impairing their characteristics as compared to samples with predominant ordered sp^3 -hybridized phase.

At the same time, SEE-characteristics of coatings are consistent with the data of Raman-spectroscopy, which is indicative of the fact that sample III is characterized by the highest ordering of the amorphous phase and the lowest percentage of polyenes in the structure. Electrical resistance of polyenes is comparable with the resistance of amorphous carbon ($\sim 10^5 \Omega \cdot \text{cm}$) [60,65]. At the same time, in the course of CVD process the polyene phase is formed mainly in the neighborhood of diamond nanoparticles [66]. Hence, the polyene component is probably a shell of diamond nanoparticles, that complicates to a significant extent the transfer of electrons because of the scattering at the phase interfaces. Thus, in the case of sample III both the ordering and the lower percentage of the polyene phase promotes the lower scattering of electrons, which increases the depth of their yield and, as a consequence, strengthens the effect of SEE.

It is worth noting that the diagnostic potential of the secondary electron emission in terms of the analysis of carbon nanostructures is not limited by different values of SEY for different energies of the primary electron beam. Secondary electrons have the typical distribution over energies (Fig. 7, a), where the following sections can be distinguished: the section of true secondary electrons (TSE region in Fig. 7, a), the region of inelastically scattered primary electrons (ISPE region in Fig. 7, a), the

region of elastically scattered primary electrons (ESPE region in Fig. 7, a) [67]. To analyze the change in the peak of elastically scattered primary electrons, a narrow energy distribution of the incident electron beam and a detector resolution of about tenths of eV are needed [68]. At the same time, the energy spectrum of true secondary electrons for different forms of carbon has features that can be detected by equipment with a resolution of about 1 eV [69,70]. The insert in Fig. 7, a shows analyzed peaks of true secondary electrons smoothed by the OriginPro software via filtration of high harmonics using fast Fourier transform.

The true secondary electron yield under electron irradiation is induced by the cascade inelastic interaction between electrons and the solid body. Therefore, the energy distribution of secondary electrons is related to the band structure of materials [69]. To show explicitly the features of secondary electron spectra, in [69,70] the energy distribution of true secondary electrons has been reconstructed in $d(N \cdot E)/dE$ coordinates from E , where N is signal intensity, E is energy of electrons. Fig. 7, b shows spectra plotted in these coordinates for the samples under study.

In [69,70] it is shown that samples with explicit bond structure, such as ordered diamond and graphite, are characterized by the presence of several explicit maxima and minima in dependencies of $d(N \cdot E)/dE$ on E . At the same time, the disordering of samples results in widening of the observed peaks and smoothing of spectral features. The trend of $III \rightarrow II \rightarrow I$ disordering growth discussed in section 3.3 is consistent with the observed change in the full width of $d(N \cdot E)/dE$ peak at half maximum ($FWHM_I = 4.9$ eV, $FWHM_{II} = 2.4$ eV, $FWHM_{III} = 1.1$ eV). However, it is worth noting that because of the composite structure of the samples, the considered dependencies are inconsistent with $d(N \cdot E)/dE$

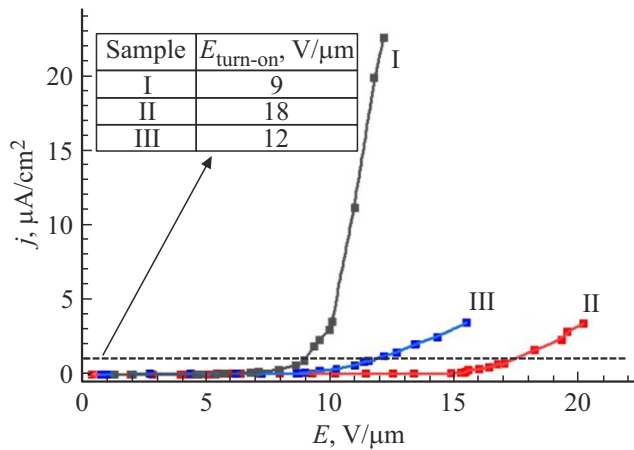


Figure 8. Voltammeteries of emission for the structures under study. Dashed line shows the current density used for the estimation of $E_{\text{turn-on}}$, the emission turn-on field. The insert shows values of $E_{\text{turn-on}}$.

characteristics for the diamond irradiated by different doses of ions [69,70] and probably they are sums of contributions from lines corresponding to different substructures.

Thus, the method of $d(N \cdot E)/dE$ analysis allows qualitative estimating of ordering of the composite a-C:ND-samples. However, when analyzing results obtained by this method, it is worth to take into account that spectrum of true secondary electrons of carbon materials may be dependent on the energy of the primary beam [71]. Also, it is worth noting that the depth of secondary electron yield is about 1–2 nm [72,73]. Therefore, the secondary electron spectra may be significantly affected by the surface oxidized/nitrogenized/hydrogenated layer, that is typical for some carbon materials [74]. In addition, carbon coatings produced by PVD methods may demonstrate formation of an sp²-rich layer saturated with the sp²-carbon to a greater extent as compared to the material volume [27,75,76],

which may have an effect on the results of surface-sensitive analysis.

3.6. Electron emission under electric field

Fig. 8 shows current-voltage emission characteristics of the samples under study. The emission turn-on field for these coatings ($E_{\text{turn-on}}$) was estimated as the field strength that makes the current density to achieve $1 \mu\text{A}/\text{cm}^2$ [77].

The emission turn-on threshold obtained for samples I, II and III was 9, 18 and $12 \text{ V}/\mu\text{m}$, respectively. These values are considerably lower than typical emission turn-on fields for polycrystalline diamond coatings without disordered phase. According to different sources, the emission turn-on field for diamond coatings may be $140 \text{ V}/\mu\text{m}$ [10], $> 60 \text{ V}/\mu\text{m}$ [78], $19\text{--}24 \text{ V}/\mu\text{m}$ [79]. Such a significant discrepancy may be due to the different morphology of materials and different sizes of crystallites, as well as to different methods of $E_{\text{turn-on}}$ estimating. As a rule, high emission turn-on threshold of diamonds is considered to be related to their significant band gap (5.5 eV) that prevents the electron transfer to the conduction band and, as a consequence, the transport of electrons [80]. At the same time, it has been shown that the presence of a conductive phase at intergrain interfaces can form conductance channels that facilitate the transfer of electrons [81]. Therefore, the emission turn-on field for nanodiamond-based samples with graphitized or carbon substructure at their intergrain interfaces is about $10\text{--}30 \text{ V}/\mu\text{m}$ [82,83]. Thus, field emission characteristics of the samples under study are in compliance with the structural attestation presented in sections 3.1–3.3 and are the evidence that under-study conditions of deposition allowed producing coatings with relatively low emission turn-on threshold.

Due to the fact that the emission of carbon materials may be caused by contributions from several mechanisms [84], this study analyzes the obtained voltammeteries by replotting them in coordinates corresponding to different mechanisms

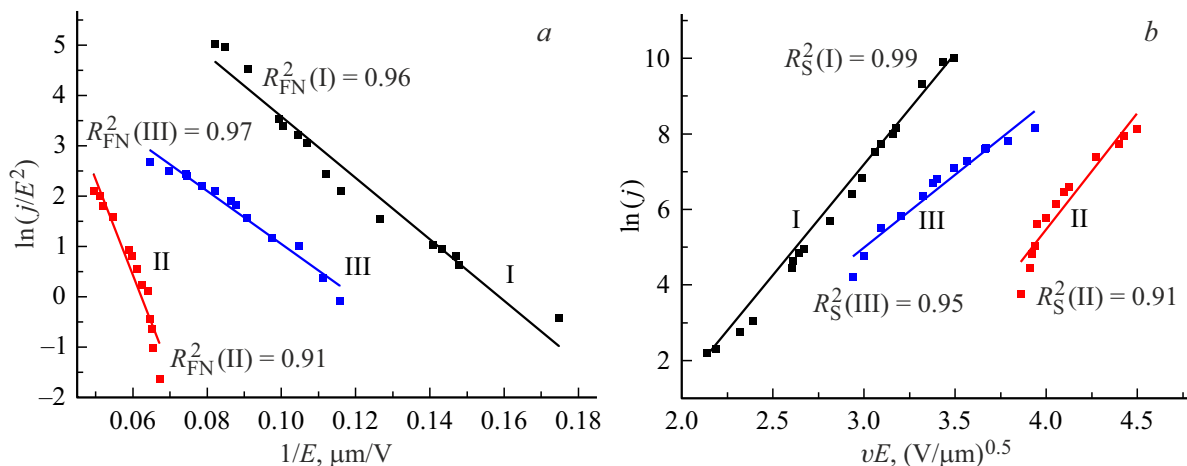


Figure 9. Voltammeteries of emission in a) Fowler–Nordheim coordinates and b) Schottky coordinates. Numbers of samples and determination coefficients for the linear approximation of experimental points in appropriate coordinates are shown.

of emission. Fig. 9, *a* shows emission characteristics of the samples under study in Fowler–Nordheim coordinates ($1/E; \ln(j/E^2)$), which are typical for the field emission. Fig. 9, *b* shows volt-amperegrams in Schottky coordinates ($\sqrt{E}; \ln(j)$), which are typical for the overbarrier emission. Coatings based on the diamond phase (including, hydrogen-passivated diamonds) and graphite-diamond composites are characterized by the field emission mechanism [10,13]. At the same time, according to [85], the thermionic emission with Schottky mechanism can contribute to the emission of polyene-containing structures, where emission is provided by the polymer component and transport of electrons is provided by a graphitized substructure.

Determination coefficients R^2 for the dependencies under study were estimated for their linear approximation in Fowler–Nordheim (R_{FN}^2) coordinates and Schottky coordinates (R_{S}^2) using the OriginPro software. This estimation shows that voltammeteries of sample I demonstrate better linearization in Schottky coordinates ($R_{\text{FN}}^2(\text{I}) = 0.96 < 0.99 = R_{\text{S}}^2(\text{III})$), although Fowler–Nordheim coordinates give better linearization for sample III ($R_{\text{FN}}^2(\text{III}) = 0.97 > 0.95 = R_{\text{S}}^2(\text{III})$). However, sample II demonstrates worse fitting of both considered dependencies ($R_{\text{FN}}^2(\text{II}) \approx R_{\text{S}}^2(\text{II}) = 0.91$). Thus, the determinative contribution for the emission of sample I is that of the Schottky mechanism, the determinative contribution for the emission of sample III is that of the field emission, and the determinative mechanism for sample II can not be identified. This result is in compliance with the data of section 3.3 showing that the percentage of polyenes in the structure decreases with the sample variation of $\text{I} \rightarrow \text{II} \rightarrow \text{III}$ and confirms the data of [85], which is indicative of the polyene phase contribution to the thermionic emission through the Schottky mechanism. In the case of sample II, probably the contributions from both mechanisms are significant making impossible the identification of the prevailing mechanism.

Emission characteristics of nanostructured samples with the diamond component are determined by both the emission of the surface layer of the material and the transport of electrons. As it has been shown in section 3.5, SEE characteristics of the samples under study are directly related to the transfer of charge carriers. Thus, it has been established that sample III has the best charge transfer characteristics, however, transport properties of I and II are adversely affected by their disordering and electron scattering at interphase interfaces between substructures of polyenes and amorphous carbon. Also, it is worth noting that, according to the data presented in section 3.3, sample I is characterized by a greater degree of hydrogen passivation of diamond nanoparticles, which decreases the work of diamond phase yield and promotes strengthening of the emission [10]. At the same time, the emission mechanism variation with the change in the percentage of the polyene component is indicative of the fact that growth of the polyene percentage in the structure can promote the emitting surface extension and have a positive effect of emission characteristics of materials.

Thus, the best emission characteristics of sample I ($E_{\text{turn-on}} = 9 \text{ V}/\mu\text{m}$) are related to the high percentage of polyenes in the structure, as well as to the hydrogen passivation of the diamond component. Sample III is characterized by the lowest hydrogen passivation and the lowest percentage of the polymer component, however, the high degree of disordering of the amorphous component and the electron scattering at interphase interfaces significantly improve the transfer of electrons, that leads to an emission turn-on field of $E_{\text{turn-on}} = 12 \text{ V}/\mu\text{m}$, which is the medium level among the samples under study. In turn, sample II is characterized by an intermediate degree of hydrogen passivation, disordering and polyene phase percentage as compared to I and III, however, its transport characteristics are comparable with those of sample I, and the percentage of the polyene component is insufficient to initiate a considerable contribution to the thermionic emission. Therefore, its emission activation field $E_{\text{turn-on}} = 18 \text{ V}/\mu\text{m}$ is the highest among the studied samples.

4. Conclusion

This study presents an analysis of the interrelation between parameters of deposition of nanostructured carbon coatings applied by CVD method, their structure and emission characteristics.

According to the X-ray diffraction data, the main component of these coatings are diamond crystallites with a size of $\sim 10 \text{ nm}$. According to the Raman-spectroscopy data, the disordered component of the film contains a phase based on the amorphous carbon, as well as several phases based on polyenes. Thus, the samples under study have a structure of a-C:ND (nanodiamonds dispersed in an amorphous carbon matrix). It has been shown, that with the decrease in the relative concentration of methane in the working chamber ($\text{I} \rightarrow \text{II}$) from 3.5 down to 2.5%, and with the increase in the relative pressure of hydrogen from 10 up to 20% for a methane pressure of 2.5% ($\text{II} \rightarrow \text{III}$) a disordering of the amorphous carbon structure takes place, the hydrogen passivation of the diamond phase decreases, and the percentage of polyene-like inclusions in the material structure becomes lower. It has been shown, that structure of the coatings synthesized at different concentrations of gases is determined by different contributions from processes of hydrocarbon deposition, hydrogen etching, ion-induced processes of defect formation and surface diffusion.

Characteristics of secondary electron emission of samples I and II are similar to those of SEE of graphite. Sample III demonstrates significantly better characteristics ($\text{SEY}_{\text{MAX}} = 2.8$ at a primary beam energy of 600 eV) due to the fact that ordering and lower percentage of the polyene phase of this coating promote lower scattering of electrons, which improves its transport characteristics and, as a consequence, strengthens the effect of SEE. The change in peak width of true secondary electrons in $d(N \cdot E)/dE$ coordinates is consistent with the disordering of the ma-

terials under study. This is indicative of the possibility of nanostructured carbon materials diagnostics through the analysis of spectrum of true secondary electrons.

The emission turn-on field obtained for samples I, II and III was 9, 18 and 12 V/ μm , respectively. The best emission characteristics of sample I are related to the hydrogen passivation of the diamond phase and the contribution of thermionic emission of the polyene substructure. Emission properties of sample III are due to its good characteristics of electron transport. No explicit contribution of hydrogen passivation and overbarrier emission is observed for sample II and SEE data is indicative of the fact that its properties related to electron transfer are worse than the transport characteristics of sample III and are comparable with properties of sample I. Therefore, sample II has the worst emission characteristics among the studied samples.

Funding

I.A. Zavidovsky acknowledges a stipend from the Theoretical Physics and Mathematics Advancement Foundation „BASIS“, grant No. 20-2-2-7-1.

Conflict of interest

The authors declare that they have no conflict of interest.

Acknowledgments

The study is carried out with the use of MicroSET-M Granit RA precision laser microprocessing with the function of 3D-structures creation purchased using the funds of the Development Program of the Lomonosov Moscow State University.

References

- [1] E.D. Eidelman, A.V. Arkhipov. *Phys. Usp.* **63**, 7, 648 (2020).
- [2] V.I. Kleshch, R.R. Ismagilov, V.V. Mukhin, A.S. Orekhov, A.S. Filatyev, A.N. Obraztsov. *Nanotechnol.* **33**, 41, 415201 (2022).
- [3] G. Kumar, H. Gupta, S. Ghosh, P. Srivastava. *Physica E* **135**, 114946 (2022).
- [4] T. Hu, S. Zhu, Y. Zhao, X. Sun, J. Yang, Y. He, X. Wang, C. Bai, H. Bai, H. Wei, M. Cao, Z. Hu, M. Liu, W. Cui. *Chin. Phys. B* **31**, 4, 047901 (2022).
- [5] H. Vázquez, A. Kononov, A. Kyritsakis, N. Medvedev, A. Schleife, F. Djurabekova. *Phys. Rev. B* **103**, 22, 224306 (2021).
- [6] M. Cao, X.-S. Zhang, W.-H. Liu, H.-G. Wang, Y.-D. Li. *Diamond. Rel. Mater.* **73**, 199 (2017).
- [7] R. Vaz, P.W. May, N.A. Fox, C.J. Harwood, V. Chatterjee, J.A. Smith, C.J. Horsfield, J.S. Lapington, S. Osbourne. *J. Inst.* **10**, 03, P03004 (2015).
- [8] M. Mastellone, A. Bellucci, M. Girolami, V. Serpente, R. Polini, S. Orlando, V. Valentini, A. Santagata, B. Paci, A. Generosi, M. Guaragno, D.M. Trucchi. *Diamond. Rel. Mater.* **128**, 109294 (2022).
- [9] M. Ficek, B. Dec, K.J. Sankaran, K. Gajewski, P. Tatarczak, I. Wlasny, A. Wysmolek, K. Haenen, T. Gotszalk, R. Bogdanowicz. *Adv. Mater. Interf.* **8**, 20, 2100464 (2021).
- [10] F. Giubileo, A. Di Bartolomeo, L. Lemmo, G. Luongo, F. Urban. *Appl. Sci.* **8**, 4, 526 (2018).
- [11] K. Panda, J.J. Hyeok, J.Y. Park, K.J. Sankaran, S. Balakrishnan, I.-N. Lin. *Sci. Rep.* **7**, 1, 16325 (2017).
- [12] M.W. Geis, J.C. Twichell, J. Macaulay, K. Okano. *Appl. Phys. Lett.* **67**, 9, 1328 (1995).
- [13] X. Jia, N. Huang, Y. Guo, L. Liu, P. Li, Z. Zhai, B. Yang, Z. Yuan, D. Shi, X. Jiang. *J. Mater. Sci. Technol.* **34**, 12, 2398 (2018).
- [14] A. Iyer, J. Etula, Y. Ge, X. Liu, J. Koskinen. *Appl. Phys. Lett.* **109**, 20, 201905 (2016).
- [15] O.A. Streletskiy, I.A. Zavidovskiy, V.V. Sychev, A.A. Dudin, S.A. Savinov, A.V. Pavlikov. *Appl. Phys. A* **128**, 1, 83 (2022).
- [16] O. Streletskiy, E. Perevedentseva, I. Zavidovskiy, A. Karmanyan, V. Sychev, V. Sadykova, A. Kuvarina, C.-L. Cheng. *Magnetochemistry* **8**, 12, 171 (2022).
- [17] R.L. Harniman, O.J.L. Fox, W. Janssen, S. Drijkoningen, K. Haenen, P.W. May. *Carbon* **94**, 386 (2015).
- [18] Y. Liu, J. He, N. Zhang, W. Zhang, Y. Zhou, K. Huang. *J. Mater. Sci.* **56**, 22, 12559 (2021).
- [19] H.P. Zhou, B. Yang, Z.D. Zhang, H. Zhang, S. Zhang, T.T. Feng, Z.Q. Xu, J. Gao, M.Q. Wu. *Appl. Surf. Sci.* **605**, 154627 (2022).
- [20] A.A. Tatarintsev, K.E. Markovets, E.I. Rau. *J. Phys. D* **52**, 11, 115104 (2019).
- [21] E.I. Rau, A.A. Tatarintsev. *Phys. Solid State* **63**, 4, 628 (2021).
- [22] T. Mōri, Y. Namba. *J. Appl. Phys.* **55**, 9, 3276 (1984).
- [23] J. Weng, F. Liu, L.W. Xiong, A. Bai, J.H. Wang. *J. Cryst. Growth* **495**, 1 (2018).
- [24] S.L. Cheng, H.C. Lin, Y.H. Huang, S.C. Yang. *RSC Adv.* **7**, 39, 23935 (2017).
- [25] A. Monshi, M.R. Foroughi, M.R. Monshi. *World J. Nano Sci. Eng.* **2**, 3, 154 (2012).
- [26] K. Hanada, T. Yoshida, Y. Nakagawa, T. Yoshitake. *Jpn J. Appl. Phys.* **49**, 12R, 125503 (2010).
- [27] O.A. Streletskiy, I.A. Zavidovskiy, V.Yu. Balabanyan, A.V. Tsiskarashvili. *Appl. Phys. A* **128**, 10, 929 (2022).
- [28] M. Rybachuk, J.M. Bell. *Carbon* **47**, 10, 2481 (2009).
- [29] M. Rybachuk, A. Hu, J.M. Bell. *Appl. Phys. Lett.* **93**, 5, 051904 (2008).
- [30] D. Ballutaud, F. Jomard, T. Kociniewski, E. Rzepka, H. Girard, S. Saada. *Diamond. Rel. Mater.* **17**, 4, 451 (2008).
- [31] F. Wang, L. Wang, Q. Xue. *Carbon* **96**, 411 (2016).
- [32] N. Wada, S.A. Solin. *Physica B+C* **105**, 1–3, 353 (1981).
- [33] J. Filik, J.N. Harvey, N.L. Allan, P.W. May, J.E.P. Dahl, S. Liu, R.M.K. Carlson. *Phys. Rev. B* **74**, 3, 035423 (2006).
- [34] A.C. Ferrari, J. Robertson. *Phys. Rev. B* **61**, 20, 14095 (2000).
- [35] J. Li, S.J. Kim, S. Han, H. Chae. *Surf. Coat. Technol.* **422**, 127514 (2021).
- [36] A. Dorner-Reisel, A. Engel, S. Svoboda, C. Schürer, S. Weißmantel. *Diamond. Rel. Mater.* **108**, 4, 107787 (2020).
- [37] T. Wu, C. Lu, T. Sun, Y. Li. *J. Mater. Sci.* **57**, 32, 15385 (2022).
- [38] G.S. Prabhakaran, R. Das, M.S.R. Rao, S.S. Bhattacharya. *Surf. Coat. Technol.* **441**, 128552 (2022).
- [39] I.A. Zavidovskiy, O.A. Streletskiy, O.Yu. Nishchak, A.A. Khaidarov, A.V. Pavlikov. *Thin Solid Films* **738**, 138966 (2021).
- [40] G. Kalita, K. Wakita, M. Umeno. *RSC Adv.* **2**, 7, 2815 (2012).
- [41] Y.A. Abdu. *Diamond. Rel. Mater.* **118**, 108536 (2021).

- [42] A.N. Obraztsov, A.V. Tyurnina, E.A. Obraztsova, A.A. Zolotukhin, B. Liu, K.-C. Chin, A.T.S. Wee. *Carbon* **46**, 6, 963 (2008).
- [43] A. Hu, Q.-B. Lu, W.W. Duley, M. Rybachuk. *J. Chem. Phys.* **126**, 15, 154705 (2007).
- [44] F.-X. Liu, K.-L. Yao, Z.-L. Liu. *Surf. Coat. Technol.* **201**, 16–17, 7235 (2007).
- [45] O.A. Streletskiy, I.A. Zavidovskiy, O.Yu. Nischak, A.V. Pavlikov. *Thin Solid Films* **671**, 31 (2019).
- [46] S.J. Askari, F. Akhtar, G.C. Chen, Q. He, F.Y. Wang, X.M. Meng, F.X. Lu. *Mater. Lett.* **61**, 11–12, 2139 (2007).
- [47] K.J. Sankaran, P.T. Joseph, H.C. Chen, N.H. Tai, I.N. Lin. *Diamond. Rel. Mater.* **20**, 2, 232 (2011).
- [48] Y.S. Kim, J.H. Lee, Y.D. Kim, S.-K. Jerng, K. Joo, E. Kim, J. Jung, E. Yoon, Y.D. Park, S. Seo, S.-H. Chun. *Nanoscale* **5**, 3, 1221 (2013).
- [49] L. Mosińska, P. Popielarski, K. Fabisiak, A. Dychalska. *Opt. Mater.* **101**, 109676 (2020).
- [50] E.I. de Obaldía, J.J. Alcantar-Peña, F.P. Wittel, J.F. Veyan, S. Gallardo-Hernandez, Y. Koudriavtsev, D. Berman-Mendoza, O. Auciello. *Appl. Sci.* **11**, 9, 3990 (2021).
- [51] O.A. Streletskiy, I.A. Zavidovskiy, O.Yu. Nischak, A.A. Haidarov. *Vacuum* **175**, 109286 (2020).
- [52] I.A. Zavidovskiy, O.Y. Nishchak, N.F. Savchenko, O.A. Streletskiy. *JETP* **134**, 6, 682 (2022).
- [53] X. Jiang, W. Beyer, K. Reichelt. *J. Appl. Phys.* **68**, 3, 1378 (1990).
- [54] W. Möller. *Appl. Phys. Lett.* **59**, 19, 2391 (1991).
- [55] C. Yang. *J. Phys.: Conf. Ser.* **2152**, 1, 012052 (2022).
- [56] K. Uppireddi, B.R. Weiner, G. Morell. *Diamond. Rel. Mater.* **17**, 1, 55 (2008).
- [57] X.-M. Tang, J. Weber, Y. Baer, C. Müller, W. Hänni, H.E. Hintermann. *Phys. Rev. B* **48**, 14, 10124 (1993).
- [58] C.Y. Vallgren, G. Arduini, J. Bauche, S. Calatroni, P. Chiggiato, K. Cornelis, P. Costa Pinto, B. Henrist, E. Métral, H. Neupert, G. Rumolo, E. Shaposhnikova, M. Taborelli. *Phys. Rev. ST Accel. Beams* **14**, 7, 071001 (2011).
- [59] Y. Kang, B. Li, J. Zhao, B. Ge, M. Weng, Z. Shi, Y. Zhao. *Vacuum* **172**, 109043 (2020).
- [60] O.A. Streletskiy, I.A. Zavidovskiy, O.Yu. Nischak, S.V. Dvoryak. *Thin Solid Films* **701**, 137948 (2020).
- [61] C.E. Nebel. *Semicond. Sci. Technol.* **18**, 3, S1 (2003).
- [62] J. Cazaux. *J. Phys. D* **38**, 14, 2442 (2005).
- [63] L.A. Gonzalez, R. Larciprete, R. Cimino. *AIP Adv.* **6**, 9, 095117 (2016).
- [64] K. Wei, S. Wu, Q. Wei, P. Zheng, W. Hu, H. Wang. *J. Electron. Mater.* **47**, 8, 4823 (2018).
- [65] C.K. Chiang, C.R. Fincher, Y.W. Park, A.J. Heeger, H. Shirakawa, E.J. Louis, S.C. Gau, A.G. MacDiarmid. *Phys. Rev. Lett.* **39**, 17, 1098 (1977).
- [66] C.-S. Wang, H.-C. Chen, H.-F. Cheng, I.-N. Lin. *J. Appl. Phys.* **107**, 3, 034304 (2010).
- [67] M.P. Seah. *Surf. Sci.* **17**, 1, 132 (1969).
- [68] M. Vos, M.R. Went. *Phys. Rev. B* **74**, 20, 205407 (2006).
- [69] A. Hoffman, S. Praver, M. Folman. *Appl. Phys. Lett.* **58**, 4, 361 (1991).
- [70] A. Hoffman, S. Praver, R. Kalish. *Phys. Rev. B* **45**, 22, 12736 (1992).
- [71] A. Modinos. *Field, Thermionic and Secondary Electron Emission Spectroscopy*. Springer, N.Y. (1984). 375 p.
- [72] W.F. van Dorp, I. Lazić, A. Beyer, A. Götz, J.B. Wagner, T.W. Hansen, C.W. Hagen. *Nanotechnol.* **22**, 11, 115303 (2011).
- [73] M.R. Scheinfein, J. Drucker, J.K. Weiss. *Phys. Rev. B* **47**, 7, 4068 (1993).
- [74] O.A. Streletskiy, O.Y. Nishchak, I.A. Zavidovskiy, K.I. Maslakov, A.V. Pavlikov. *Thin Solid Films* **739**, 138993 (2021).
- [75] M.A. Caro, V.L. Deringer, J. Koskinen, T. Laurila, G. Csányi. *Phys. Rev. Lett.* **120**, 16, 166101 (2018).
- [76] S. Wang, K. Komvopoulos. *Sci. Rep.* **11**, 1, 3914 (2021).
- [77] S. Park, A.P. Gupta, S.J. Yeo, J. Jung, S.H. Paik, M. Mativenga, S.H. Kim, J.H. Shin, J.S. Ahn, J. Ryu. *Nanomater.* **8**, 6, 378 (2018).
- [78] W.J. Zhang, Y. Wu, W.K. Wong, X.M. Meng, C.Y. Chan, I. Bello, Y. Lifshitz, S.T. Lee. *Appl. Phys. Lett.* **83**, 16, 3365 (2003).
- [79] W.-E. Chen, C. Chen, C.-J. Yeh, X. Hu, K.-C. Leou, I.-N. Lin, C.-R. Lin. *ACS Appl. Mater. Interfaces* **10**, 34, 28726 (2018).
- [80] W. Zhu, G.P. Kochanski, S. Jin, L. Seibles. *J. Appl. Phys.* **78**, 4, 2707 (1995).
- [81] K.J. Sankaran, S. Kunuku, K.-C. Leou, N.-H. Tai, I.-N. Lin. *ACS Appl. Mater. Interfaces* **6**, 16, 14543 (2014).
- [82] C.-J. Yeh, H.-T. Chang, K.-C. Leou, I.-N. Lin. *Diamond. Rel. Mater.* **63**, 197 (2016).
- [83] K.Y. Teng, H.C. Chen, H.Y. Chiang, C.C. Horng, H.F. Cheng, K.J. Sankaran, N.H. Tai, C.Y. Lee, I.N. Lin. *Diamond. Rel. Mater.* **24**, 126 (2012).
- [84] P.W. May, M.-T. Kuo, M.N.R. Ashfold. *Diamond. Rel. Mater.* **8**, 8–9, 1490 (1999).
- [85] O.A. Streletskiy, I.A. Zavidovskiy, O.Y. Nishchak, A.A. Haidarov, N.F. Savchenko, A.V. Pavlikov. *JETP* **135**, 6, 844 (2022).

Translated by Y.Alekseev